linear optical susceptibilities," *Phys. Rev. Lett.*, vol. 22, pp. 787–790, 1969.
——"A new contribution to the nonlinear optical susceptibility arising from inequal atomic radii," *Phys. Rev. Lett.*, vol. 25, pp. 440–443, 1970.
——, "Calculations of nonlinear optical susceptibilities in a wide range of compounds," *IEEE J. Quantum Electron.* (Corresp.), vol. QE-8, pp. 609–610, Sept. 1972.
——, "Bond charge calculation of nonlinear optical susceptibilities for various crystal structures," *Phys. Rev. B*, Mar. 1973.
[4] R. C. Miller, "Optical second harmonic generation in piezoelectric crystals," *Appl. Phys. Lett.*, vol. 5, pp. 17–19, 1964.
[5] That is, those not containing an atom in the first periodic row.
[6] S. K. Suri, H. K. Henish, and J. W. Faust, Jr., "Growth of β-AgI single crystals in gels," *J. Cryst. Growth*, vol. 7, pp. 277–281, 1970.
[7] J. Jerphagnon and S. K. Kurtz, "Maker fringes: A detailed comparison of theory and experiment for isotropic and uniaxial crystals," *J. Appl. Phys.*, vol. 41, pp. 1667–1681, 1970.
[8] Landolt-Börnstein, *Zahlenwerte und Funktionen*, vol. 2, pt. 8. Berlin: Springer, 1962.
[9] The bulk and surface scattering losses at 2ω were 34 and 27 percent, respectively.
[10] B. F. Levine and C. G. Bethea, "Nonlinear susceptibility of GaP; relative measurement and use of measured values to determine a better absolute value," *Appl. Phys. Lett.*, vol. 20, pp. 272–275, 1972.
[11] R. C. Miller and W. A. Nordland, "Absolute signs of nonlinear optical coefficients of polar crystals," vol. 1, pp. 400–402, 1970.
[12] A. S. Bhalla, S. K. Suri, and E. W. White, "Crystallographic polarity of gel grown β-AgI crystals," *J. Appl. Phys.*, vol. 42, pp. 1833–1835, 1971.
[13] N. Bloembergen and P. S. Pershan, "Light waves at the boundary of nonlinear media," *Phys. Rev.*, vol. 128, pp. 606–622, 1962.
[14] F. G. Parsons, E. Y. Chen, and R. K. Chang, "Dispersion of nonlinear optical susceptibilities in hexagonal II–VI semiconductors," *Phys. Rev. Lett.*, vol. 27, pp. 1436–1439, 1971.
[15] F. N. H. Robinson, "Relations between the components of the nonlinear polarizability tensor in cubic and hexagonal II–VI compounds," *Phys. Lett.*, vol. 26A, pp. 435–436, 1968.
[16] The wurtzite Δ_{33} and the zinc blende Δ_{14} are simply related by $\Delta_{33} = (2/\sqrt{3})\Delta_{14}$.

Optical Third-Harmonic Generation in Alkali Metal Vapors

RICHARD B. MILES AND STEPHEN E. HARRIS

Abstract—**This paper considers third-harmonic generation in phase-matched mixtures of alkali metal vapors and inert gases. Calculations show that the combination of near-resonant nonlinear susceptibilities, the ability to phase match, and the relatively high UV transparency of these vapors should allow high conversion efficiency for picosecond laser pulses with a peak power of 10^8-10^9 W. Calculations of the nonlinear susceptibility and of the ratio of xenon atoms to metal vapor atoms which is necessary to achieve phase matching are given for each of the alkalies as a function of incident laser wavelength. Processes that limit the allowable peak power density and energy density are discussed and guides for determining the metal vapor pressure, cell length, and beam area are given.**

I. Introduction

THIS PAPER presents a theoretical analysis of phase-matched optical third-harmonic generation in alkali metal vapors. Calculations predict the efficient conversion of high-power picosecond laser pulses into the ultraviolet. Three complementary phenomena combine to produce the potentially high conversion efficiency: 1) resonant nonlinear susceptibility, 2) phase matching, and 3) ultraviolet transparency.

The resonant enhancement of the third-harmonic nonlinear susceptibility arises from resonant denominators at the first, second, and third harmonics of the incident frequency. Susceptibilities of the alkalies in the visible and near-infrared spectral region are typically five orders of magnitude greater than those of the inert gases in the same region. The conversion efficiency is proportional to the square of this susceptibility.

Phase matching is possible because alkali metal vapors are anomalously dispersive if the driving frequency is chosen below and its third harmonic chosen above the primary resonance line. A normally dispersive buffer gas such as xenon may be added to vary the indices of refraction until both the first and third harmonics travel at the same velocity through the gas mixture. Third-harmonic generation then becomes cumulative over the entire length of the gas cell and a substantial increase of the power conversion is possible.

The small absorption cross sections of the alkali vapors above their ionization potentials assure that the third harmonic is not reabsorbed by the vapor itself. This ultraviolet transparency allows generation to spectral regions that are not accessible to nonlinear optical crystals.

Assuming that high efficiencies can be experimentally realized, third-harmonic generation in gas mixtures will have a number of significant advantages over third-harmonic generation or sequential second-harmonic generation in nonlinear crystals. Nonlinear crystal

Manuscript received October 25, 1972. This work was supported jointly by the U. S. Air Force Cambridge Research Laboratories, the Office of Naval Research, NASA, and the U. S. Army Research Office, and by a grant to R. B. Miles from the Fannie and John K. Hertz Foundation.

R. B. Miles is with the Department of Aerospace and Mechanical Sciences, Engineering Quadrangle, Princeton, N. J. 08540.
S. E. Harris is with the Hansen Microwave Laboratory, Stanford University, Stanford, Calif. 94305.

transparency is now limited to below the cutoff of ammonium dihydrogen phosphate at about 2000 Å, while gases have no such limitation. The isotopic nature of gas mixtures eliminates Poynting vector walkoff characteristic of birefringent phase matching in crystals. Breakdown power and energy densities are higher in gases and breakdown does not destroy the medium. Gas cells may ultimately be made with very large apertures to handle large incident optical energies.

Conversely, metal vapor tripling cells are not nearly as simple and will be more expensive than nonlinear crystals. Even theoretically, the required incident power is much higher for efficient tripling in vapors than for efficient doubling in crystals. At this time the highest experimental conversion efficiency obtained in metal vapors is about 10^{-4}, and considerable experimental effort will be necessary to attempt to verify the calculations and predictions of this paper.

In the following sections, the third-harmonic nonlinear susceptibility is calculated and plotted as a function of wavelength for each of the alkalies. Tables of matrix elements, oscillator strengths, and transition energies are given. The power conversion equation is developed and the ratio of xenon atoms to alkali atoms, which is necessary to obtain phase matching, is given for each of the alkalies. Experimental results confirm the calculation of the susceptibility to within 15 percent and correlate almost perfectly with the theoretical phase-matching behavior.

Processes that limit the maximum metal vapor density, and thus the maximum conversion efficiency, are discussed. These include: single and multiphoton absorption and ionization, Kerr effect, breakdown, thermal defocusing, and breaking of the phase-matching condition as a result of atomic saturation. Typically this latter process will be the most severe and will probably limit the energy density to about 1 J/cm² for tripling 1.064-μ radiation. Formulas for determining the metal vapor pressure, cell length, and beam area are given.

Before proceeding, we note that third-harmonic generation in the inert gases has been extensively studied by Ward and New [1]. The concept of phase matching by gas mixing was suggested by Armstrong *et al.* [2]. The metal vapor inert gas system was proposed by Harris and Miles [3], and demonstrated by Young *et al.* [4].

II. Calculation of the Susceptibility

Third-harmonic light is generated from a radiating power-density-dependent third-harmonic component of the induced polarization. For high power densities, this third-harmonic nonlinearity becomes large and radiation may be substantial. The creation of the third-harmonic component can be visualized as a step-by-step process beginning with a strong electric field that interacts with ground state electrons and produces an induced dipole moment at the driving frequency. This induced dipole moment interacts with the field to create a 2ω variation of excited and mixed state populations. These populations again interact with the field to produce a third-harmonic component of the dipole moment. These interactions occur simultaneously and no transitions are involved.

If the incident electric field is written as

$$\mathcal{E}(t, r) = \tfrac{1}{2}[\mathcal{E}(r)e^{-i\omega t} + \mathcal{E}^*(r)e^{i\omega t}], \tag{1}$$

we can define the polarization at the third-harmonic frequency as

$$\mathcal{P}^{(3)}(t, r) = \tfrac{1}{2}[\mathcal{P}^{(3)}(r)e^{-i3\omega t} + \mathcal{P}^{(3)*}(r)e^{i3\omega t}] \tag{2}$$

where

$$\mathcal{P}^{(3)}(r) = \frac{N\chi^{(3)}(3\omega)[\mathcal{E}(r)]^3}{4} \tag{3}$$

and N is the density of atoms/cubic centimeter. Armstrong *et al.* [2] have shown $\chi^{(3)}(3\omega)$ to be given by

$$\chi^{(3)}(3\omega) = \frac{1}{\hbar^3}\sum_g \sum_{a,b,c} \mu_{ga}\mu_{ab}\mu_{bc}\mu_{cg}\rho_{gg}A_{abc}, \tag{4}$$

where μ_{ij} are the dipole matrix elements, ρ_{gg} is the probability of occupancy of the ground level, and A_{abc} are frequency factors:

$$\begin{aligned} A_{abc} = {} & \frac{1}{(\Omega_{ag} - 3\omega)(\Omega_{bg} - 2\omega)(\Omega_{cg} - \omega)} \\ & + \frac{1}{(\Omega_{ag} + \omega)(\Omega_{bg} + 2\omega)(\Omega_{cg} + 3\omega)} \\ & + \frac{1}{(\Omega_{ag} + \omega)(\Omega_{bg} + 2\omega)(\Omega_{cg} - \omega)} \\ & + \frac{1}{(\Omega_{ag} + \omega)(\Omega_{bg} - 2\omega)(\Omega_{cg} - \omega)} \end{aligned} \tag{5}$$

where Ω_{ij} are the atomic transition frequencies. We assume the incident laser field to be linearly polarized in the z direction and thus take $\mu_{ij} = e\langle i\,|z|\,j\rangle$.

The Hamiltonian from which the eigenstates $|i\rangle$ are derived includes a term describing the $L - S$ coupling that is characteristic of the alkalies and other multielectron atoms. This coupling accounts for the splitting of the energy levels with quantum numbers L greater than zero and is responsible, for instance, for the two closely separated sodium D lines. If the driving frequency is much farther from the resonances than the splitting, the $L - S$ coupling may be neglected by replacing the split resonance lines with an average resonance. Angular and spin eigenstates then become identical to those of the hydrogen atom. The radial quantum number n, however, must be derived from the particular alkali's radial wavefunctions. Equation (6) results from ignoring the $L - S$ coupling and is used for the ensuing calculations:

$$\begin{aligned} \chi^{(3)}(3\omega) = {} & \frac{e^4}{\hbar^3}\sum_{a,b,c} \{\langle g\ s\ 0\ \tfrac{1}{2}\ |z|\ a\ p\ 0\ \tfrac{1}{2}\rangle\langle a\ p\ 0\ \tfrac{1}{2}\ |z|\ b\ s\ 0\ \tfrac{1}{2}\rangle \\ & \cdot\langle b\ s\ 0\ \tfrac{1}{2}\ |z|\ c\ p\ 0\ \tfrac{1}{2}\rangle\langle c\ p\ 0\ \tfrac{1}{2}\ |z|\ g\ s\ 0\ \tfrac{1}{2}\rangle A_{ap,bs,cp} \\ & + \langle g\ s\ 0\ \tfrac{1}{2}\ |z|\ a\ p\ 0\ \tfrac{1}{2}\rangle\langle a\ p\ 0\ \tfrac{1}{2}\ |z|\ b\ d\ 0\ \tfrac{1}{2}\rangle \\ & \cdot\langle b\ d\ 0\ \tfrac{1}{2}\ |z|\ c\ p\ 0\ \tfrac{1}{2}\rangle\langle c\ p\ 0\ \tfrac{1}{2}\ |z|\ g\ s\ 0\ \tfrac{1}{2}\rangle A_{ap,bd,cp}\}. \end{aligned} \tag{6}$$

TABLE I
MATRIX ELEMENTS OF THE ALKALIES

Lithium

Transition	f	ΔE(Ry)	$\langle z \rangle$ (Bohr Radii)	Transition	f	ΔE(Ry)	$\langle z \rangle$ (Bohr Radii)
2s-2p	0.744	0.1359	-2.34	2p-3d	0.635	0.1494	2.26
2s-3p	0.00428	0.2020	0.123	2p-4d	0.122	0.1980	0.860
2s-4p	0.00398	0.3325	0.109	2p-5d	0.0462	0.2206	0.501
2s-5p	0.00239	0.3557	0.082	2p-6d	0.0229	0.2328	0.345
3s-2p	- 0.327	- 0.1122	1.71	3p-3d	0.0742	0.0033	5.23
3s-3p	1.21	0.0339	- 5.97	3p-4d	0.521	0.0519	3.47
3s-4p	0.0000364	0.0845	- 0.021	3p-5d	0.130	0.0745	1.45
3s-5p	0.00125	0.1077	0.108	3p-6d	0.0543	0.0867	0.867
4s-2p	- 0.0378	- 0.1833	0.454	4p-3d	- 0.302	- 0.0473	0.876
4s-3p	- 0.667	- 0.0373	4.23	4p-4d	0.136	0.0014	-10.76
4s-4p	1.64	0.0133	-11.11	4p-5d	0.490	0.0240	4.95
4s-5p	0.000990	0.0365	- 0.165	4p-6d	0.132	0.0362	2.09
5s-2p	- 0.0127	- 0.2133	0.244	5p-3d	- 0.00530	- 0.0705	0.314
5s-3p	- 0.0775	- 0.0672	1.07	5p-4d	- 0.0735	- 0.0218	2.01
5s-4p	- 1.01	- 0.0167	7.78	5p-5d	0.191	0.00076	-17.37
5s-5p	2.05	0.0055	-17.74	5p-6d	0.487	0.0130	6.70

Potassium

Transition	f	ΔE(Ry)	$\langle z \rangle$ (Bohr Radii)	Transition	f	ΔE(Ry)	$\langle z \rangle$ (Bohr Radii)
4s-4p	1.04	0.11875	-2.96	4p-3d	0.839	0.07760	3.60
4s-5p	0.0154	0.22534	-0.261	4p-4d	0.00121	0.13105	0.105
4s-6p	0.00277	0.26446	-0.102	4p-5d	0.00163	0.15647	-0.112
4s-7p	0.000968	0.28352	-0.0585	4p-6d	0.00226	0.17025	-0.126
5s-4p	-0.525	-0.07297	2.68	5p-3d	-0.234	-0.02899	-3.11
5s-5p	1.50	0.03362	-6.68	5p-4d	1.19	0.02446	7.64
5s-6p	0.0316	0.07274	-0.659	5p-5d	0.00779	0.04988	0.433
5s-7p	0.00602	0.09160	-0.256	5p-6d	0.0000153	0.06366	-0.0170
6s-4p	-0.0500	-0.13154	0.617	6p-3d	-0.0110	-0.06811	-0.440
6s-5p	-0.957	-0.02495	6.19	6p-4d	-0.502	-0.01466	-6.41
6s-6p	1.94	0.01417	-11.7	6p-5d	1.51	0.01076	12.98
6s-7p	0.0499	0.03303	- 1.23	6p-6d	0.0159	0.02454	0.882
7s-4p	-0.0164	-0.15728	0.323	7p-3d	-0.00317	-0.08697	0.209
7s-5p	-0.0810	-0.05069	1.26	7p-4d	-0.0324	-0.03352	-1.08
7s-6p	-1.37	-0.01157	10.88	7p-5d	-0.762	-0.00810	-10.62
7s-7p	2.37	0.00729	-18.03	7p-6d	1.82	0.00568	19.61

Sodium

Transition	f	ΔE(Ry)	$\langle z \rangle$ (Bohr Radii)	Transition	f	ΔE(Ry)	$\langle z \rangle$ (Bohr Radii)
3s-3p	0.972	0.1547	-2.51	3p-3d	0.855	0.1113	-3.04
3s-4p	0.0153	0.2760	-0.235	3p-4d	0.0996	0.1603	-0.864
3s-5p	0.00251	0.3195	-0.0886	3p-5d	0.0311	0.1830	-0.452
3s-6p	0.000821	0.3401	-0.0491	3p-6d	0.0140	0.1953	-0.293
4s-3p	-0.502	-0.0800	2.51	4p-3d	-0.195	-0.0100	4.83
4s-4p	1.44	0.0413	-5.90	4p-4d	0.948	0.0390	-5.40
4s-5p	0.0385	0.0848	-0.677	4p-5d	0.142	0.0617	-1.66
4s-6p	0.00779	0.1054	-0.272	4p-6d	0.0493	0.0740	-0.894
5s-3p	-0.0412	-0.1480	0.528	5p-3d	-0.000275	-0.0535	-0.079
5s-4p	-0.937	-0.0267	5.92	5p-4d	-0.382	-0.0045	10.09
5s-5p	1.88	0.0168	-10.58	5p-5d	1.05	0.0182	- 8.32
5s-6p	0.0620	0.0374	- 1.29	5p-6d	0.173	0.0305	- 2.61
6s-3p	-0.0131	-0.1769	0.272	6p-3d	-0.0000517	-0.0741	- 0.0289
6s-4p	-0.0696	-0.0556	1.12	6p-4d	-0.00141	-0.0251	- 0.260
6s-5p	-1.36	-0.0121	10.59	6p-5d	-0.558	-0.0024	16.80
6s-6p	2.31	0.0084	-16.56	6p-6d	1.17	0.0099	-11.88

Rubidium

Transition	f	ΔE(Ry)	$\langle z \rangle$ (Bohr Radii)	Transition	f	ΔE(Ry)	$\langle z \rangle$ (Bohr Radii)
5s-5p	1.09	0.1161	-3.06	5p-4d	0.594	0.0604	3.44
5s-6p	0.0243	0.2167	-0.335	5p-5d	0.0273	0.1182	-0.526
5s-7p	0.00535	0.2540	-0.145	5p-6d	0.0233	0.1455	-0.438
5s-8p	0.00209	0.2721	-0.0876	5p-7d	0.0144	0.1600	-0.329
6s-5p	-0.562	-0.0674	2.89	6p-4d	-0.141	-0.0402	-2.05
6s-6p	1.54	0.0331	-6.82	6p-5d	0.935	0.0177	7.97
6s-7p	0.0412	0.0704	-0.765	6p-6d	0.0182	0.0449	-0.698
6s-8p	0.00883	0.0886	-0.316	6p-7d	0.0172	0.0594	-0.589
7s-5p	-0.0525	-0.1238	0.650	7p-4d	-0.0115	-0.0775	-0.422
7s-6p	-1.00	-0.0232	6.56	7p-5d	-0.331	-0.0196	-4.50
7s-7p	1.98	0.0141	-11.85	7p-6d	1.23	0.0076	13.95
7s-8p	0.0613	0.0322	- 1.38	7p-7d	0.0122	0.0221	- 0.814
8s-5p	-0.0172	-0.1487	0.340	8p-4d	-0.00353	-0.0957	0.210
8s-6p	-0.0808	-0.0481	1.30	8p-5d	-0.0350	-0.0378	- 1.06
8s-7p	-1.42	-0.0108	11.48	8p-6d	-0.521	-0.0106	- 7.69
8s-8p	2.40	0.0074	-18.06	8p-7d	1.50	0.0040	21.29

The eigenstates in the equation above are $|n\ l\ m_l m_s\rangle$, where $m_l = l, l-1, \cdots, -l$, and $m_s = \pm\frac{1}{2}$. Selection rules for the dipole z-matrix elements state that $\Delta l = \pm 1, \Delta m_l = 0$, $\Delta m_s = 0$ [5]. These differ from the total dipole matrix-element selection rules that include x and y components and also allow $\Delta m_l = \pm 1$.

The ground state of the alkalies, for which $l = 0$, is indicated by $n = g$, $l = s$, and it is assumed that this is the only populated level. We see from the selection rules that the energy levels associated with $n = a$ and $n = c$ in (6) must be p levels ($l = 1$). Those associated with $n = b$ may be either s levels ($l = 0$) or d levels ($l = 2$). Thus (6) has two terms: those for which the b levels are s states, and those for which the b levels are d states. The $A_{ap,bd,cp}$ factor is the frequency factor of (5) with resonances Ω between $|ap\rangle$ and ground, $|bd\rangle$ and ground, and $|cp\rangle$ and ground.

Values for the dipole matrix elements in terms of l and m values and the radial $\mathfrak{R}$ factor are given in Slater [6]. For the z component

$$\langle n\ l\ m_l\ |z|\ n'l+1\ m_l\rangle = \sqrt{(l+1)^2 - m_l^2}\ \mathfrak{R}_{nl;n'l+1}, \quad (7)$$

where

TABLE I
CONTINUED

Cesium

Transition	f	ΔE(Ry)	$\langle z \rangle$ (Bohr Radii)	Transition	f	ΔE(Ry)	$\langle z \rangle$ (Bohr Radii)
6s-6p	1.13	0.1053	-3.28	6p-5d	0.197	0.0275	2.93
6s-7p	0.0270	0.1996	-0.368	6p-6d	0.281	0.1009	-1.83
6s-8p	0.00631	0.2349	-0.164	6p-7d	0.0902	0.1323	-0.904
6s-9p	0.00255	0.2523	-0.101	6p-8d	0.0407	0.1484	-0.574
7s-6p	-0.576	-0.0637	3.01	7p-5d	-0.0240	-0.0668	-0.657
7s-7p	1.58	0.0306	-7.19	7p-6d	0.354	0.0066	8.00
7s-8p	0.0401	0.0659	-7.80	7p-7d	0.203	0.0381	-2.99
7s-9p	0.00862	0.0833	-0.322	7p-8d	0.0933	0.0541	-1.44
8s-6p	-0.0565	-0.1164	0.670	8p-5d	-0.00284	-0.1022	-0.183
8s-7p	-1.02	-0.0222	6.78	8p-6d	-0.0955	-0.0207	-2.00
8s-8p	2.01	0.0132	-12.34	8p-7d	0.470	0.0027	14.45
8s-9p	0.0580	0.0305	- 1.38	8p-8d	0.255	0.0187	- 4.27
9s-6p	-0.0189	-0.1401	0.367	9p-5d	-0.000854	-0.1195	- 0.0926
9s-7p	-0.0858	-0.0458	1.37	9p-6d	-0.0156	-0.0461	- 0.638
9s-8p	-1.44	-0.0105	11.73	9p-7d	-0.0173	-0.0147	- 3.76
9s-9p	2.43	0.0069	-18.78	9p-8d	0.578	0.00138	22.42

$$\mathcal{R}_{nl;n'l+1} = \frac{1}{\sqrt{(2l+1)(2l+3)}} \int_0^\infty r^3 R_{nl} R_{n'l+1}\, dr \qquad (8)$$

and R_{nl} is the radial wave function.

The matrix elements to be used in (6) for calculation of the third-harmonic nonlinear susceptibility include only states with $m_l = 0$. Thus we find

$$\langle n\ l\ 0\ |z|\ n'l+1\ 0\rangle = (l+1)\mathcal{R}_{nl;n'l+1}. \qquad (9)$$

Values for this matrix element may be found from the Bates and Damgaard [7] approach, which assumes a Coulombic radial potential field and tabulates the values of the radial function in terms of the effective quantum number of each level. They define σ, which is $e\mathcal{R}$ in our notation. The sign of $\mathcal{R}$ is important and is included in their derivation; however, Bebb [8] mentions a sign error of $(-1)^{(n-n')+1}$ in his work.

An alternative, and perhaps superior, approach to the evaluation of matrix elements is to find their absolute value from tabulated oscillator strengths and the sign from Bates and Damgaard. Solving for the matrix element $\langle n\ l\ 0 \cdot |z|\ n'l+1\ 0\rangle$ in terms of the oscillator strength yields

$$|\langle n\ l\ 0\ |z|\ n'l+1\ 0\rangle|^2 = f_{nl;n'l+1} \frac{\hbar}{2m_e\Omega_{n'l+1;nl}} \frac{3(l+1)}{2l+3}, \qquad (10)$$

where $f_{nl;n'l+1}$ is the oscillator strength, $\hbar\Omega_{n'l+1;nl}$ is the energy difference associated with the $|n\ l\ 0\rangle$ to $|n'l+1\ 0\rangle$ transition, and m_e is the electron mass. If the resonant frequency Ω is written as an energy difference in rydbergs and the matrix element is found in Bohr radii, then

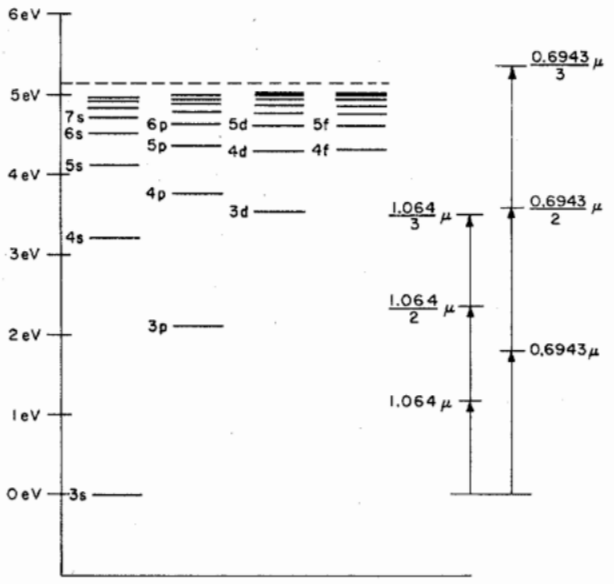

Fig. 1. Energy levels of sodium.

$$|\langle n\ l\ 0\ |z|\ n'l+1\ 0\rangle| = \sqrt{\frac{f_{nl;n'l+1}}{E_{n'l+1} - E_{nl}} \frac{3(l+1)}{2l+3}}. \qquad (11)$$

The average frequency factors to be used in (6) are calculated from the $L - S$ split levels weighted by the relative line strengths:

$$\begin{aligned} \tfrac{2}{3}E_{np(j=3/2)} + \tfrac{1}{3}E_{np(j=1/2)} &= E_{np} \\ \tfrac{2}{5}E_{nd(j=3/2)} + \tfrac{3}{5}E_{nd(j=5/2)} &= E_{nd}. \end{aligned} \qquad (12)$$

The average energy levels are used in Table I to give allowed transition energies between the lowest four s, p, and d states for each of the alkalies. These 12 levels create 128 terms in the summation and constitute our approximation of the nonlinear susceptibility.

Fig. 1 shows the average energy levels of sodium. It is apparent that the approximation is not good for driving frequencies whose first, second, or third harmonic is above the levels used and below the ionization potential. Continuum absorption is small for the alkalies and is neglected in this derivation. Table I gives the $\langle n\ l\ 0\ |z|n'l+1\ 0]$ matrix elements with the oscillator strengths and energy differences from which they are calculated. For consistency, these oscillator strengths have all been taken from calculations by Anderson [9], [10]. The signs of the matrix elements are from Bates and Damgaard with the correction factor mentioned by Bebb.

Figs. 2–6 give $|\chi^{(3)}(3\omega)|$ in electrostatic units versus wavelength for each of the alkalies. The regions where our approximation does not include resonant levels are marked as invalid. Substantial cancellations from the signs of both frequency factors and matrix elements account for the numerous zeros. It is important to note that the 2ω resonances (occurring with the excited s or d levels) do not correspond to allowed single photon absorption, and, if approached by 2ω, could be used to enhance the third-harmonic susceptibility without substantially increasing the loss at the fundamental frequency.

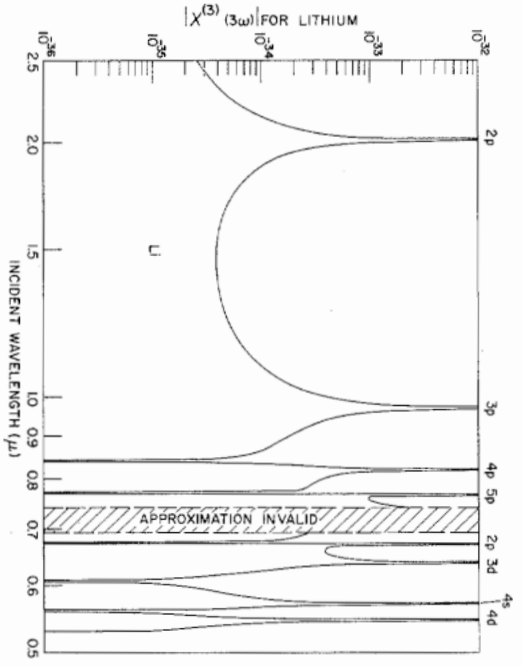

Fig. 2. Nonlinear susceptibility of lithium versus incident wavelength.

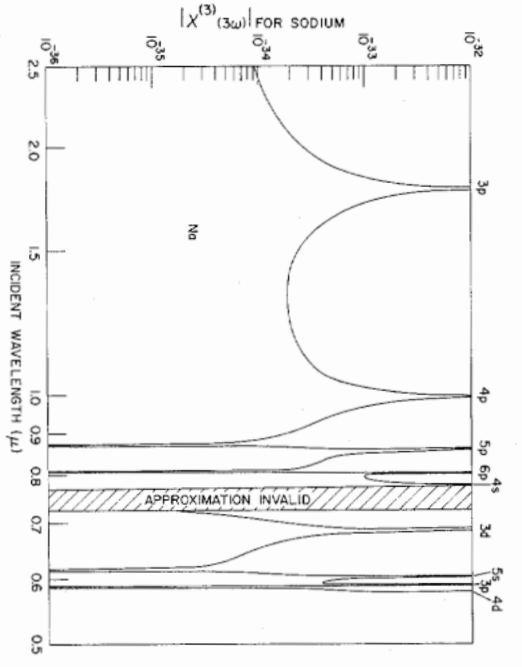

Fig. 3. Nonlinear susceptibility of sodium versus incident wavelength.

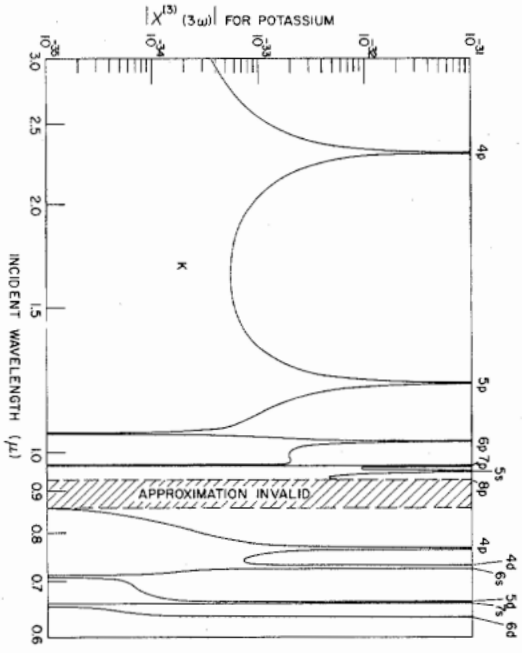

Fig. 4. Nonlinear susceptibility of potassium versus incident wavelength.

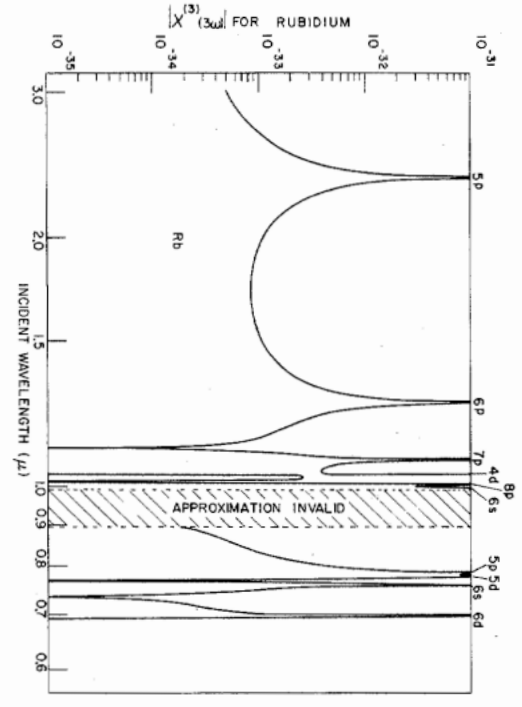

Fig. 5. Nonlinear susceptibility of rubidium versus incident wavelength.

III. Third-Harmonic Power Conversion

We assume the incident electric field to be a TEM_{00} Gaussian mode focused at $z = f$ with a confocal beam parameter b. Then

$$\mathcal{E}(r) = \mathcal{E}_0 e^{ik_1 z}(1 + i\xi)^{-1} \exp\left[-k_1(x^2 + y^2)/b(1 + i\xi)\right]. \quad (13)$$

In this expression $k_1 = 2\pi n_1/\lambda$, where n_1 is the index of refraction at the incident wavelength λ; $b = 2\pi w_0^2/\lambda$, where w_0 is the beam radius; and $\xi = 2(z - f)/b$. From Ward and New [1], the generated third-harmonic electric field is given by

$$\mathcal{E}^{(3)}(r) = \left[i \tfrac{1}{16} \eta c k_0^2 b N \chi^{(3)}(3\omega) \mathcal{E}_0^2 / k_3\right] \cdot \exp\left[3ik_1 z\right](1 - i\xi)^{-1} \cdot I(\Delta k, \xi, \zeta) \exp\left(-\frac{3k_1(x^2 + y^2)}{b(1 + i\xi)}\right) \quad (14)$$

where

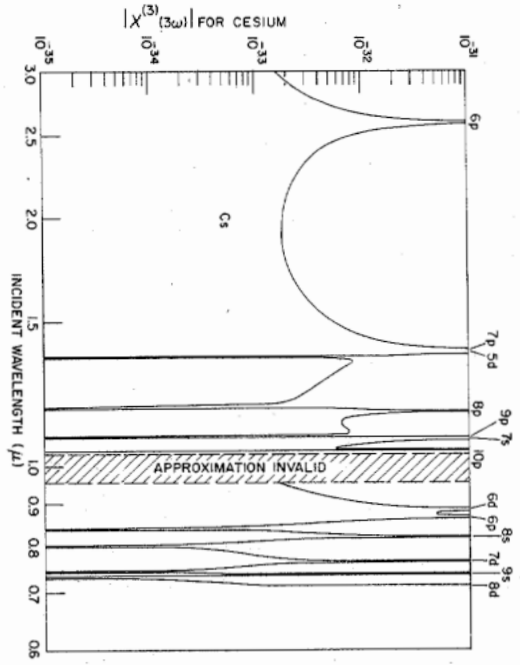

Fig. 6. Nonlinear susceptibility of cesium versus incident wavelength.

$$I(\Delta k, \xi, \zeta) = \int_{-\zeta}^{\xi} d\xi' \frac{\exp\left[\frac{1}{2} i b \Delta k (\xi - \xi')\right]}{(1 + i\xi')^2} \tag{15}$$

and

k_0 $= 6\pi/\lambda$,
k_3 $= n_3 k_0$,
n_3 index of refraction at the third harmonic,
N number of atoms/cubic centimeter,
η $= \sqrt{\mu_0/\epsilon_0} \cong 377$,
$\chi^{(3)}(3\omega)$ $= (1/81 \times 10^{-17})\chi^{(3)}(3\omega)_{\text{ESU}}$,
ξ $= 2(L - f)/b$,
ζ $= 2f/b$,
L length of the gas cell,
f location of the beam focus from the entrance window,
Δk $= k_3 - 3k_1 = \frac{6\pi}{\lambda}(n_3 - n_1)$ = wave-vector mismatch.

All units of length are in centimeters.

The third-harmonic power is obtained by integrating over r, and in terms of the incident power $P^{(1)}$, is

$$P^{(3)} = \frac{3\eta^4\pi^2c^2}{\lambda^4} N^2[\chi^{(3)}(3\omega)]^2 |I(\Delta k, \xi, \zeta)|^2 [P^{(1)}]^3. \tag{16}$$

The conversion efficiency is defined as the ratio of third- to first-harmonic power. With the power in watts, the alkali atom density N in atoms/cubic centimeter, the nonlinear coefficient $\chi^{(3)}(3\omega)$ in ESU, and the incident wavelength λ in centimeters, the conversion efficiency becomes

$$\frac{P^{(3)}}{P^{(1)}} = \frac{8.215 \times 10^{-2}}{\lambda^4} N^2[\chi^{(3)}(3\omega)]^2 |I|^2 [P^{(1)}]^2. \tag{17}$$

The integral I accounts for the effects of focusing and dispersion. Two limiting regimes of (17) are of interest. In the plane-wave approximation ($b >> L$), I^2 reduces to $(4L^2/b^2)\,\text{sinc}^2(\Delta kL/2)$. Using $A = b\lambda/4$, where A is the effective area of the Gaussian beam, (17) becomes

$$\frac{P^{(3)}}{P^{(1)}_{(\text{plane wave})}} = \frac{5.134 \times 10^{-3}}{\lambda^2} N^2L^2[\chi^{(3)}(3\omega)]^2 \cdot \text{sinc}^2\left(\frac{\Delta kL}{2}\right)\left[\frac{P^{(1)}}{A}\right]^2. \tag{18}$$

On the other hand, tight focusing in the center of the cell ($b << L$, $\xi = \zeta$) gives

$$|I|^2_{(\text{tight focusing})} = [\pi b \Delta k \exp(+\tfrac{1}{2} b\Delta k)]^2, \tag{19}$$

for $\Delta k < 0$ and $|I|^2 = 0$ for $\Delta k \geq 0$.

For the plane-wave approximation, maximum conversion efficiency is attained with $\Delta k = 0$. In the tight focusing approximation for negatively dispersive media, conversion efficiency is maximized for $b\Delta k = -4$. For confocal focusing ($b = L$, $\xi = \zeta$) at the center of a negatively dispersive media, $|I|^2$ maximizes at 2.46 when $\Delta kL = -3.5$.

A. Phase Matching

For the condition where the confocal parameter is much longer than the gas cell, i.e., the plane-wave approximation, Δk must be made equal to zero. If two gases are mixed together, one with a negative and the other with positive dispersion, then at some ratio of partial pressures, Δk will be zero and phase matching will occur. It thus suffices to mix some nonreactive gas, such as xenon, with the alkali vapor to phase match. In the absence of this buffer gas, the third-harmonic generation only occurs over the short distance that the first and third harmonics overlap. This is called the coherence length and is $L_c = |\pi/\Delta k|$. Phase matching will increase this interaction length to the length of the cell and thus increase the output power by a factor of $(\pi L/2L_c)^2$. The refractive index of a phase-matched Rb and Xe mixture is shown in Fig. 7. Note that the partial pressures have been chosen so that the index at the third harmonic equals that at the fundamental.

The refractive index of the metal vapors is calculated from the standard Sellmeier equation

$$n - 1 = \frac{Nr_e}{2\pi} \sum_i \frac{f_i}{[(1/\lambda_i^2) - (1/\lambda^2)]}, \tag{20}$$

where

r_e $= 2.818 \times 10^{-13}$ cm,
f_i oscillator strength of the ith transition,
λ_i wavelength of the ith transition in centimeters.

Values of the f_i and λ_i for Li, Na, K, Rb, and Cs are given in Table V. The refractive index of Xe is taken from Koch [11], who derived the following equation from experimental data at STP:

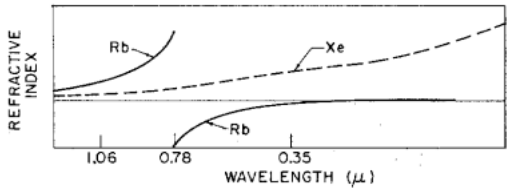

Fig. 7. Refractive indices of rubidium and xenon versus wavelength.

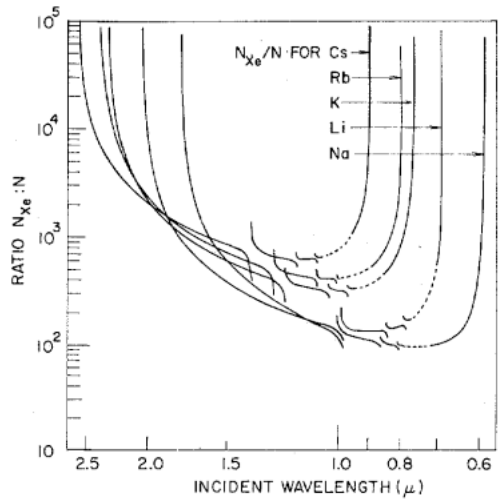

Fig. 8. Required ratio of Xe to alkali atoms versus incident wavelength for phase-matched third-harmonic generation.

$$n_{Xe} - 1 \cong \left\{\frac{393235}{46.3012 - 10^{-8}/\lambda^2} + \frac{393235}{59.5779 - 10^{-8}/\lambda^2} + \frac{7366100}{139.8310 - 10^{-8}/\lambda^2}\right\} \times 10^{-8} \quad (21)$$

where λ is in centimeters. Fig. 8 plots the ratio of the number of Xe to alkali atoms versus the incident wavelength for phase-matched third-harmonic generation in each of the alkalies.

When picosecond pulses are used for third-harmonic generation, it is necessary that the broad frequency spectrum that comprises the pulse be simultaneously phase matched; or equivalently that the fundamental and third harmonic maintain at least 50-percent temporal overlap. The minimum allowable pulse length $\Delta t_{\min}$, which satisfies this condition, is determined by the difference in group velocities Δv_g of the fundamental and third harmonic, and is given by

$$\Delta t_{\min} = \frac{n_1 n_3 L}{c^2}\left[\frac{\partial \omega_3}{\partial k_3} - \frac{\partial \omega_1}{\partial k_1}\right] = \frac{n_1 n_3 \Delta v_g}{c^2} L = BL. \quad (22)$$

The term $(n_1 n_3 \Delta v_g)/c^2$ is labeled B and is proportional to the density of atoms; the normalized constant B/N is given in Table II for 1.064- and 0.6943-μ tripling experiments. From these data we see that 50 cm of Rb vapor at 10^{17} atoms/cm^3 will phase match a 0.17-ps or longer pulse of 1.064-μ radiation. This is to be compared with a minimum pulse time of 6.1 ps for a 1-cm crystal of $LiNbO_3$ and 0.07 ps for a 1-cm crystal of KDP for doubling 1.064-μ radiation [12].

TABLE II
PARAMETERS FOR THIRD-HARMONIC GENERATION

Element	$\chi^{(3)}(3\omega)$ [ESU]	L_cN	Ratio $N_{Xe}:N$	B/N
		1.064 μ To 0.3547 μ		
Li	1.25×10^{-34}	9.79×10^{16}	154	1.80×10^{-30}
Na	-3.93×10^{-34}	5.86×10^{16}	152	2.77×10^{-32}
K	2.61×10^{-34}	2.73×10^{16}	326	1.81×10^{-32}
Rb	6.15×10^{-33}	2.15×10^{16}	414	3.30×10^{-32}
Cs	-1.17×10^{-32}	1.39×10^{16}	658	5.36×10^{-32}
		0.6943 μ To 0.2314 μ		
Li	3.00×10^{-34}	5.03×10^{16}	400	1.93×10^{-30}
Na	3.16×10^{-34}	2.01×10^{16}	100	3.69×10^{-32}
K	6.17×10^{-35}	9.60×10^{15}	---	---
Rb	8.23×10^{-34}	9.94×10^{15}	---	---
Cs	3.25×10^{-33}[a]	1.65×10^{16}	---	---

[a] Includes extra energy levels that are near the 0.6943-μ resonance.

Table II presents other relevant data for the 1.064- and 0.6943-μ conversion experiments. Li and Na are the only alkalies that phase match 0.6943 μ; thus the ratio of xenon to alkali atoms and B/N are given only for those two vapors. The coherence length is inversely proportional to the density of alkali atoms and is tabulated as L_cN, which may be derived from (20).

The density of atoms of each alkali is calculated from the vapor pressure. A good approximation of the vapor pressure for pressures near 1 mmHg is

$$p(\text{mm}) \cong \exp[-(a/T) + d], \quad (23)$$

where the constants a and d are given in Table III for each of the alkalies and T is the temperature in degrees Kelvin. The density of atoms is, then,

$$N = 9.66084 \times 10^{18} \frac{p(\text{mm})}{T} \text{ atoms/cm}^3. \quad (24)$$

As the temperature and thus the density of alkali atoms increase, the allowed temperature tolerance necessary to maintain phase matching decreases. A maximum allowed variation on Δk of $\delta(\Delta k) = \pi/L$ yields a maximum allowed temperature variation of

$$\delta(T) = \frac{L_c}{L} T\left[\frac{a}{T} - 1\right]^{-1}, \quad (25)$$

where a is the constant in Table III. A temperature of 814 K gives 10^{17} atoms of Na. From Tables II and III, L_c is 5.86×10^{-1} cm and $a = 1.2423 \times 10^4$. These numbers yield $\delta(T) = 33.4/L$ K, where L is in centimeters. Typically the vapor pressure will be low because of other limiting processes and the temperature tolerance will be no problem.

B. Tight Focusing

In the tight focus regime ($b \ll L$), setting $\Delta kb = -4$ maximizes the conversion efficiency. As opposed to the

TABLE III
VAPOR PRESSURE CONSTANTS

	Li	Na	K	Rb	Cs
a	19571.4	12423.3	10210.4	9140.07	8827.58
d	19.130	17.391	16.539	16.0628	16.0007

TABLE IV
THIRD-HARMONIC GENERATION BY TIGHT FOCUSING

Element	$N_{\text{tight focusing}}$ (atoms/cm^3)	K
	1.064 μ To 0.3547 μ	
Li	$7.37 \times 10^{16}/b$	1.11×10^{-28}
Na	$7.46 \times 10^{16}/b$	1.13×10^{-27}
K	$3.47 \times 10^{16}/b$	1.08×10^{-28}
Rb	$2.75 \times 10^{16}/b$	3.75×10^{-26}
Cs	$1.72 \times 10^{16}/b$	5.31×10^{-26}
	0.6943 μ To 0.2314 μ	
Li	$6.40 \times 10^{15}/b$	1.14×10^{-29}
Na	$2.56 \times 10^{16}/b$	2.02×10^{-28}

plane-wave condition where the sinc^2 function is identical for positive or negative Δk, the integral is only nonzero for negative Δk in the tight focus approximation and thus a negatively dispersive medium is necessary. Since the wave-vector mismatch Δk is proportional to N, the number of atoms/cubic centimeter required for maximum conversion by tight focusing is

$$N_{\text{tight focusing}} = 4(L_c N)/b\pi. \tag{26}$$

Substituting this value of N into (17), we obtain

$$\frac{P^{(3)}}{P_{\text{tight focusing}}^{(1)}} = K(P/A)^2. \tag{27}$$

Values of $N_{\text{tight focusing}}$ and K are given in Table IV for tripling 1.064- and 0.6943-μ radiation.

Though this type of phase matching is of interest because of its simplicity, it is likely that multiphoton absorption [8], [22] will limit the allowable incident power density to about 10^{11} W/cm^2 and thus (in Cs, for instance) will limit the maximum conversion efficiency to about 5.31×10^{-4}.

Fig. 9 shows calculated third-harmonic power versus temperature for a beam confocally focused ($b = L$) into a 10-cm cell filled with Rb vapor and a similar experiment using an imaginary vapor with the same characteristics as Rb except positively dispersive. The difference is easily noted and provides a method of distinguishing positively from negatively dispersive media. The large first peak occurs only if Δk is negative and equal to $-3.5/L$.

C. Experimental Results

Experimental results have been presented elsewhere [4]. A recent correction of the theory yielded experimental verification of the nonlinear susceptibility to within 15 percent. Third-harmonic conversion of 1.064–0.3547 μ in a Rb and xenon mixture is reproduced in Fig. 10 together with the theoretical prediction. To achieve the best experimental–theoretical fit, it was necessary to translate the experimental points by 5°C. The peak at 267°C corresponds to the temperature at which the rubidium vapor density was in the proper ratio to the xenon density to cause phase matching.

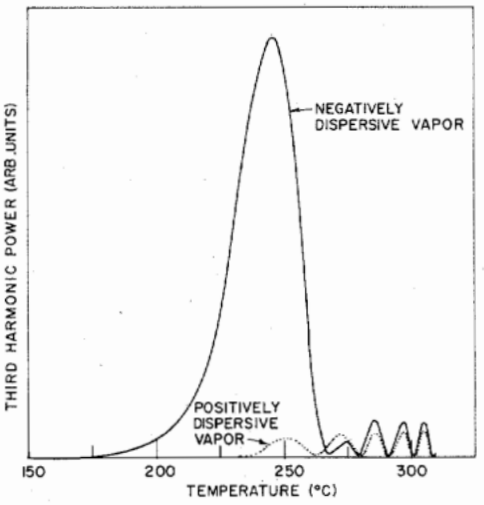

Fig. 9. Third-harmonic output from a negatively and positively dispersive vapor with the incident beam confocally focused into a 10-cm cell.

IV. LIMITING PROCESSES

Third-harmonic generation is limited at high powers and high-power densities by competing processes. Absorption will, of course, deplete the pump or the third-harmonic radiation. Off line center, however, absorption is generally not as severe a problem as are saturation (with the associated breaking of phase matching and self focusing), multiphoton absorption, and gas breakdown. Other processes will cause additional refractive index variations and the dominant limiting process depends on the particular experimental configuration.

A. Absorption

The single-photon absorption cross section is

$$\sigma^{(1)}(\omega) = \frac{\pi e^2 \eta \omega}{\hbar} |\langle f | z | g \rangle|^2 \rho(\omega). \tag{28}$$

Third-harmonic generation will most likely be done in relatively high-pressure gas cells and far off single-photon absorption resonances. Since the Lorentzian line shape decreases much slower off resonance than does the Gaussian and also characterizes pressure broadening,

$$\rho(\omega) = \frac{1}{\pi} \left\{ \frac{2\,\Omega_{fg}\,\omega\Delta\omega}{[\Omega_{fg}^2 - \omega^2]^2 + (\omega\Delta\omega)^2} \right\}, \tag{29}$$

where $\Delta\omega$ is the Lorentzian broadened full width at the half-power points.

The single-photon cross section may also be expressed

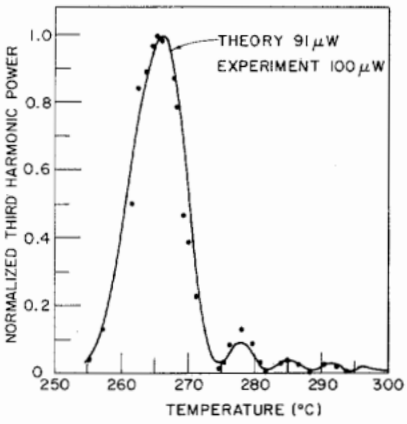

Fig. 10. Third-harmonic power output from rubidium vapor phase matched with xenon: theory and experiment.

in terms of the oscillator strength of the $g \rightarrow f$ transition. If we let $\omega = 2\pi c\nu$, where ν is in centimeter^{-1}, c is in centimeters/second, and use (29) for the line shape, the cross section far off line center becomes

$$\sigma^{(1)}(\omega) \cong 2r_e f_{gf} \frac{\nu^2 \Delta\nu}{[\nu_{fg}^2 - \nu^2]^2}. \tag{30}$$

Measurements of the pressure-broadened linewidth of alkali gases in argon are tabulated by Ch'en and Takeo [13] and show that the line width is proportional to the relative density of the gas. Relative density is the pressure of the same number of atoms at 0°C; thus the pressure-broadened linewidth is proportional to the number of buffer gas atoms present.

More generally, the linewidth must include contributions from natural, or lifetime, broadening and from self-broadening effects. If the number of buffer gas atoms is R times the number of alkali atoms, where R is determined by the phase-matching criterion, the Lorentzian linewidth is

$$\Delta\nu = \Delta\nu_{\text{natural}} + \delta\nu_s N/N_0 + \delta\nu R N/N_0. \tag{31}$$

$\delta\nu$ is the pressure broadened, $\delta\nu_s$ is the self-broadened linewidth at standard temperature and pressure, and $N_0 = 2.69 \times 10^{19}$ atoms/cm^3. Values for $\Delta\nu_{\text{natural}}$, $\delta\nu_S$, and $\delta\nu$ are given in Table V for the absorption lines of the alkalies. The numbers for $\delta\nu$ enclosed in parentheses are estimates; the other numbers of $\delta\nu$ are taken from Ch'en and Takeo's tables for argon broadening and are only approximately correct for broadening with xenon. Oscillator strengths are taken from the sources referenced and do not necessarily correspond to those from which the matrix elements given in Table I were derived. There, for the sake of consistency, Anderson's calculations were used exclusively. The resonant wavelengths are from Landolt and Bornstein [14].

The natural width is calculated from the natural lifetime, or quenching time [18],

$$\tau_c = 1.51 \left(\frac{g_f}{g_g}\right) \frac{\lambda_{fg}^2}{f_{gf}}, \tag{32}$$

TABLE V
ABSORPTION LINE PARAMETERS

Element	Resonance (μ)	f	$\delta\nu_s$ (cm^{-1})	$\delta\nu^a$ (cm^{-1})	τ_c (s)	$\Delta\nu_N$ (cm^{-1})
Li [10]	0.6708	0.744	36.8	(0.72)	2.7×10^{-8}	1.9×10^{-4}
	0.3234	0.00428	0.10	(2.5)	1.1×10^{-6}	4.8×10^{-6}
	0.2742	0.00398	0.081	(2.5)	8.6×10^{-5}	6.2×10^{-6}
Na [15]	0.5892	0.982	42.7	0.72	1.6×10^{-8}	3.3×10^{-4}
	0.3303	0.0142	0.35	(2.5)	3.5×10^{-7}	1.5×10^{-5}
	0.2853	0.0022	0.046	(2.5)	1.7×10^{-6}	3.1×10^{-6}
K [15]	0.7676	1.04	59.0	1.01	2.5×10^{-8}	2.1×10^{-4}
	0.4045	0.0154	0.46	2.5	4.8×10^{-7}	1.1×10^{-5}
	0.3447	0.00277	0.071	(2.5)	2.0×10^{-6}	2.7×10^{-6}
Rb [16]	0.7948	0.395	69.6	0.627	2.4×10^{-8}	2.2×10^{-4}
	0.7800	0.805	69.6	0.855	2.3×10^{-8}	2.3×10^{-4}
	0.4216	0.00532	0.50	2.21	5.0×10^{-7}	1.1×10^{-5}
	0.4202	0.01068	0.50	2.56	5.0×10^{-7}	1.1×10^{-5}
	0.3592	0.000979	0.078	(2.56)	2.0×10^{-6}	2.7×10^{-6}
	0.3587	0.00196	0.078	(2.56)	2.0×10^{-6}	2.7×10^{-6}
Cs [17]	0.8944	0.394	78.1	(0.627)	3.1×10^{-8}	1.7×10^{-4}
	0.8521	0.814	76.9	(0.855)	2.7×10^{-8}	2.0×10^{-4}
	0.4593	0.00284	0.29	1.63	1.1×10^{-6}	4.8×10^{-6}
	0.4555	0.0174	0.88	2.22	3.5×10^{-7}	1.5×10^{-5}
	0.3890	0.000517	0.027	2.69	7.3×10^{-6}	7.3×10^{-7}
	0.3876	0.00349	0.15	2.69	1.3×10^{-6}	4.0×10^{-6}

[a] Values of $\delta\nu$ in parentheses are estimates; others are from Ch'en and Takeo [13].

by

$$\Delta\nu_N = \frac{1}{2\pi c\tau_c}. \tag{33}$$

g_g and g_f are degeneracies of the lower- and upper-energy levels and λ_{fg} is the transition wavelength in centimeters. Values for τ_c are included in Table V and are important for the saturation process discussed in the following section. The self-broadened linewidth $\delta\nu_s$ is calculated from the relation [19]

$$\delta\nu_s = \frac{3 \times 6^{1/2}}{4\pi} \frac{r_e \lambda_{fg} f_{gf}}{g_f} N_0. \tag{34}$$

For convenience we will ignore the self-broadened and natural linewidths in (31) when calculating the pressure-broadened cross section. The error will not be large since typical values of R are greater than 100 and the xenon pressure-broadened linewidths are only approximate.

Table VI gives values of $\sigma^{(1)}(\omega)/N$ for tripling 1.064 and 0.6943 μ in the alkali vapors phase matched with xenon. Single-photon cross sections at the third harmonic, $\sigma^{(1)}(3\omega)/N$, and two-photon cross sections, $\sigma^{(2)}(\omega)/N$, are included as well. The single-photon cross section at the third harmonic corresponds to the absorption of the generated third harmonic. For tripling 0.6943 μ, $\sigma^{(1)}(3\omega)$ is derived from the continuum cross section and is assumed independent of N. The absorption coefficient is, of course, $\alpha = N\sigma L$, and forms an upper limit on the length and density of the gas cell.

Single-photon absorption to the continuum is of con-

TABLE VI
SINGLE- AND TWO-PHOTON ABSORPTION CROSS SECTIONS (σ IN cm^2, N IN ATOMS/cm^3, P/A IN W/cm^2)

Element	Ratio $N_{Xe}:N$	Phase Matched With Xe $\sigma^{(1)}(\omega)/N$	$\sigma^{(1)}(3\omega)/N$	$\sigma^{(2)}(\omega)/N$
		1.064–0.3547 μ		
Li	154	8.5×10^{-39}	5.4×10^{-39}	$9.2 \times 10^{-52} P/A$
Na	152	5.0×10^{-39}	1.3×10^{-38}	$1.8 \times 10^{-51} P/A$
K	326	9.6×10^{-38}	3.9×10^{-38}	$2.6 \times 10^{-49} P/A$
Rb	414	1.3×10^{-37}	1.8×10^{-37}	$1.1 \times 10^{-42} P/A$
Cs	658	5.7×10^{-37}	1.0×10^{-37}	$2.2 \times 10^{-46} P.A$
Element	Ratio $N_{Xe}:N$	$\sigma^{(1)}(\omega)/N$	$\sigma^{(1)}(3\omega)$[a]	$\sigma^{(2)}(\omega)/N$
		0.6943–0.2314 μ		
Li	400	4.3×10^{-36}	2.5×10^{-18}	$2.2 \times 10^{-47} P/A$
Na	100	4.7×10^{-38}	8.0×10^{-20}	$8.3 \times 10^{-48} P/A$

[a] Continuum absorption cross section from Ditchburn [20] assumed independent of N.

cern if the third-harmonic frequency is above the ionization potential of the alkali atom, as is the case for tripling 0.6943 μ. A summary of measurements is presented by Ditchburn *et al.* [20]. It shows that the cross sections of the alkalies are typically less than 10^{-18} cm^2. Sodium, for example, has a cross section of 1.2×10^{-19} cm^2 at its ionization threshold. The cross section then drops to 2×10^{-20} at 0.1900 μ and rises slowly toward higher frequencies. This behavior is typical of alkalies and indicates that the generated third-harmonic signal will not be significantly absorbed if it is above the ionization energy. The Kuhn–Thomas sum rule predicts this low absorption since the sum of the discrete level oscillator strengths is very nearly 1 for all the alkalies.

At pressures of a few torr, the alkali metal vapors contain from 1 to 10 percent diatomic molecules. The absorption bands are diffuse and the value of the absorption cross sections in the IR and UV do not appear to have been determined.

Preliminary experimental measurements in our laboratory indicate, at least at pressures of a few torr for tripling of 1.064 μ in Na vapor, that molecular absorption should not be a problem. If the fundamental or third-harmonic frequency should fall in the middle of a molecular band, it is likely that the molecular absorption will bleach very rapidly and will not affect the refractive index as much as atomic absorption. The absence of knowledge of molecular absorption is a weak point of this paper and requires experimental study.

A derivation of the two-photon cross section to discrete levels is given by Bebb [21]. With the matrix elements in Bohr radii, the power density in watts/centimeters^2, and the resonant and incident energies in rydbergs (1 Ry = 109 737.31 cm^{-1}),

$$\sigma^{(2)}(\omega) = 4.597 \times 10^{-34} \cdot \left| \sum_{a_1} \frac{\langle f \,|z|\, a_1\rangle\langle a_1 \,|z|\, g\rangle}{E_{a_1,g} - E} \right|^2 \omega\rho(2\omega) \frac{P}{A} \text{ cm}^2. \quad (35)$$

The lineshape is again Lorentzian.

Values of the two-photon absorption cross section for tripling 1.064 and 0.6943 μ are given in Table VI. The linewidth used for these calculations is $\delta^{(2)}\nu = 2.7$ cm^{-1} and represents an approximation of the widths of the upper d and s levels. For typical conditions away from resonances, two-photon absorption can be ignored.

Morton [22] has derived multiple-photon ionization transition probabilities for the alkalies for incident wavelengths of 1.059, 0.6943, 0.5295, and 0.3472 μ. The multiple-photon absorption cross section is found from these transition probabilities by the relation

$$\sigma^{(q)} = \frac{q\hbar\omega W}{P/A} \quad (36)$$

where q is the number of photons absorbed and W is the transition probability in second^{-1}. Values for $\sigma^{(q)}$ are given in Table VII. It is likely that multiphoton ionization will be the dominant process that limits the allowable power density, and at typical pressures and cell lengths this ionization will limit this density to about 10^{10} or 10^{11} W/cm^2. Once high efficiency is reached, multiple-photon ionization caused by the generated third-harmonic radiation may further restrict the allowable incident power density.

B. Saturation

The energy density that is applied in a time less than the quenching time and that reduces the ground state population by e^{-1} is termed the saturation energy density:

$$J_{sat}/A = \frac{\hbar\Omega_{fg}}{2\sigma^{(1)}(\omega)}. \quad (37)$$

If the energy is applied in a time longer than the quenching time τ_c, then the pulse length is no longer of importance and the saturation power density becomes

$$P_{sat}/A = \frac{\hbar\Omega_{fg}}{2\sigma^{(1)}(\omega)\tau_c}. \quad (38)$$

The saturation energy density can be written in terms of

TABLE VII
MULTIPLE-PHOTON IONIZATION CROSS SECTIONS[a]

	1.059 μ	0.6943 μ	0.5295 μ	0.3472 μ
Li	6.8×10^{-66} (P/A)^4	7.8×10^{-50} (P/A)^3	6.4×10^{-42} (P/A)^2	1.9×10^{-30} (P/A)
Na	2.2×10^{-65} (P/A)^4	3.4×10^{-40} (P/A)^2	6.3×10^{-41} (P/A)^2	3.2×10^{-30} (P/A)
K	1.7×10^{-52} (P/A)^3	3.3×10^{-41} (P/A)^2	1.4×10^{-30} (P/A)	5.8×10^{-29} (P/A)
Rb	7.5×10^{-51} (P/A)^3	2.7×10^{-39} (P/A)^2	1.8×10^{-30} (P/A)	1.9×10^{-30} (P/A)
Cs	3.7×10^{-49} (P/A)^3	3.9×10^{-39} (P/A)^2	3.8×10^{-30} (P/A)	3.8×10^{-28} (P/A)

[a] From Morton [22].

the cross-section off line center given in (29):

$$J_{sat}/A = \frac{hc[\nu_{fg}^2 - \nu^2]^2}{4 r_e f_{of} \nu \Delta\nu}. \tag{39}$$

The linewidth depends on the total density of atoms; if it is below about 10^{16} atoms/cm^3, then the natural linewidth is to be used (see Table V); for higher pressures, the expression of (31) gives the linewidth. Pressure broadening is generally anticipated, so

$$J_{sat}/A = 4.74 \times 10^8 \frac{[\nu_{fg}^2 - \nu^2]^2}{f_{of} \nu \delta\nu R N} \text{ J/cm}^2. \tag{40}$$

The saturation energy density is maximized when the total density of atoms is so low that the natural linewidth dominates. The first two columns of Table VIII give this maximum saturation energy density and J_{sat}/A as given by (40) for tripling of 1.064- and 0.6493-μ radiation.

Though J_{sat}/A is comfortably large, a more severe limitation is imposed on the allowable incident energy density by the tolerance on the phase-matching condition and by thermal defocusing. For $J/A \ll J_{sat}/A$, the fractional variation in atomic population δN is

$$\frac{\delta N}{N} = \frac{J/A}{J_{sat}/A}. \tag{41}$$

We may accept a half-power tolerance on the phase-matching condition $\delta(\Delta k)$ of

$$\delta(\Delta k)_{alk} L = \pi. \tag{42}$$

The coherence length L_c of the alkali vapor is defined as

$$\Delta k_{alk} L_c = \pi. \tag{43}$$

Assuming that only the alkali vapor experiences saturation and noting that both $\delta(\Delta k_{alk})$ and Δk_{alk} are proportional to the atomic population, then

$$\frac{\delta(\Delta k_{alk})}{\Delta k_{alk}} = \frac{\delta N}{N} = \frac{L_c}{L}. \tag{44}$$

Equation (44) is somewhat in error since it neglects the contribution of excited atoms to the refractive index. This error depends on the particular alkali and incident wavelength and is generally less than a factor of 2. Combining the above equations, we obtain the maximum allowable incident energy density that will not break the phase-matching condition as

TABLE VIII
SATURATION DENSITY IN PHASE-MATCHED GAS MIXTURES (J/A IN J/cm^2, N IN ATOMS/cm^3, L IN cm)

Element	Maximum J_{sat}/A	$(J_{sat}/A) \times N$	$(J_{phase\ matching}/A) \times N^2$
	1.064–0.3547 μ		
Li	2.37×10^5	1.09×10^{19}	$6.39 \times 10^{35}/L$
Na	2.29×10^5	1.88×10^{18}	$1.09 \times 10^{36}/L$
K	5.64×10^4	9.77×10^{17}	$2.67 \times 10^{34}/L$
Rb	4.14×10^4	7.14×10^{17}	$1.54 \times 10^{34}/L$
Cs	1.77×10^4	1.62×10^{18}	$2.22 \times 10^{33}/L$
	0.6943–0.2314 μ		
Li	1.84×10^3	3.28×10^{16}	$1.67 \times 10^{32}/L$
Na	2.47×10^4	2.99×10^{18}	$5.76 \times 10^{34}/L$
K	8.05×10^3	—	—
Rb	1.03×10^4	—	—
Cs	3.11×10^4	—	—

[a] Assumes natural linewidth in (39).

$$J_{phase\ matching}/A = \frac{L_c}{L} (J_{sat}/A). \tag{45}$$

Values for this quantity are given in the third column of Table VIII. Since both L_c and J_{sat} vary as $(1/N)$, $J_{phase\ matching}/A$ varies as $1/N^2$. In general, this quantity will impose the most severe limitation on the allowable incident energy density.

Saturation of the alkali metal vapor may also lead to thermal focusing or defocusing of the incident beam. For a Gaussain beam profile the variation of refractive index across the beam is

$$n(x) \cong n_0 - \delta n + \delta n \frac{2x^2}{w_0^2}, \tag{46}$$

where w_0 is the beam radius and $\delta n = n_0(J/A)/(J_{sat}/A)$. We assume a beam with its waist at the center of the cell and a complex beam parameter q_0 [23]. The ray transfer matrix is

$$\begin{bmatrix} A & B \\ C & D \end{bmatrix} = \begin{bmatrix} 1 & L \\ \frac{4\delta n L}{w_0^2} & 1 \end{bmatrix}, \tag{47}$$

which yields a q_0 at the cell exit of

$$q_1 = \frac{q_0 + (L/2)}{(2\delta n L/w_0^2) q_0 + 1}. \tag{48}$$

The beam waist at the cell exit is then

$$w_1^2(L/2) = \left(\frac{\lambda}{\pi}\right)^2\left[\frac{L^2/4 + (\pi^2 w_0^4/\lambda^2)}{w_0^2 - \delta n L^2}\right]. \quad (49)$$

Normalization to the beam waist in absence of thermal defocusing ($\delta n = 0$) gives the ratio

$$\frac{w_1^2(L/2)_{\text{focusing}}}{w_1^2(L/2)_{\text{no focusing}}} = \frac{1}{(w_0^2 - \delta n L^2)/(1/w_0^2)}. \quad (50)$$

If we assume that a rough criterion for significant thermal defocusing is that this ratio = 2, then

$$\delta n_{\text{allowable}} = \frac{w_0^2}{2L^2}, \quad (51)$$

and

$$\frac{\delta N}{N} = \frac{\delta n}{n} = \frac{w_0^2}{2L^2 n} = \frac{3L_c}{L^2}\frac{w_0^2}{\lambda}. \quad (52)$$

For confocal focusing, $w_0^2 = (L\lambda/2\pi)$ and

$$\frac{\delta N}{N} = \frac{3}{2\pi}\left(\frac{L_c}{L}\right), \quad (53)$$

which differs from the tolerance imposed by the breaking of phase matching (44) by a factor of $3/2\pi$.

C. Breakdown

Gas breakdown at high optical intensities appears to be a two-step process. Initially a small number of free electrons are created in the focal volume through multiple-photon ionization. These electrons then gain energy through inverse bremsstrahlung absorption of radiation and collide with atoms to create more free electrons in an avalanche process that finally leads to an opaque plasma.

Kishi *et al.* [24] have found that free electrons are created at much lower power intensities than observed breakdown thresholds, indicating that only the avalanche process need be analyzed. The theoretical threshold power density for inverse bremsstrahlung behaves as [24], [25]

$$\left(\frac{P}{A}\right)_{\text{breakdown}} \approx \frac{\omega^2}{N}\left(\frac{1}{t_p} + \frac{1}{\tau_b}\right) \quad (54)$$

where t_p is the laser pulse length. The steady-state response time τ_b is determined by whatever competing loss process is dominant: at high pressures, electrons lose energy from elastic collisions and at low pressures the electrons diffuse very rapidly away from the focal volume. Observations of breakdown in air by Wang and Davis [26] yield τ_b on the order of $\frac{1}{2}$ ns. Krasyuk *et al.* [27], however, find that their results with picosecond pulses in inert gases scale approximately by $1/t_p$ to measurements done with 30-ns lasers.

Rizzo and Klewe [28] have measured the breakdown thresholds of Rb and Cs. Although the vapor densities were low, they observed a behavior characteristic of the avalanche processes. Their results show that a 65-ns ruby laser pulse breaks down 10^{16} atoms/cm^3 at a focal density of about 10^{10} W/cm^2, and that breakdown threshold varies as $1/N$. It seems likely that with picosecond pulses, $t_p \ll \tau_b$ and that breakdown is determined by energy density (as opposed to power density). Furthermore, the maximum energy density that is allowed by the stringent condition on the breaking of phase matching will almost certainly be less than that which will cause gas breakdown.

TABLE IX
QUADRATIC KERR SUSCEPTIBILITY

Element	$\chi^{(3)}(\omega)$ (ESU)	Kerr Effect[a] (W/cm^2)
	1.064–0.3547 μ	
Li	6.7×10^{-34}	2.0×10^{12}
Na	8.2×10^{-34}	1.6×10^{12}
K	1.7×10^{-32}	8.0×10^{10}
Rb	6.9×10^{-32}	2.0×10^{10}
Cs	-2.1×10^{-31}	6.3×10^{9}
	0.6943–0.2314 μ	
Li	3.2×10^{-32}	2.8×10^{10}
Na	6.3×10^{-32}	1.4×10^{10}
K	-2.8×10^{-32}	3.2×10^{10}
Rb	-3.0×10^{-32}	3.0×10^{10}
Cs	1.5×10^{-22}	6.0×10^{10}

[a] Assumes 10^{16} atoms/cm^3 and a 1-m cell.

D. Quadratic Kerr Effect

The contribution of the third-order nonlinear susceptibility to the polarization at the driving frequency causes a change in refractive index that may also break phase matching and cause focusing or defocusing of the incident laser beam. The third-order polarization at ω is derived similarly to the third-harmonic polarization of (3) and leads to a variation of the refractive index as a function of incident power density given by

$$\delta n = \frac{\eta N \chi^{(3)}(\omega)(P/A)}{4\epsilon_0}. \quad (55)$$

Given N in atoms/cubic centimeter, χ in ESU, and P/A in watts/square centimeters, the variation of index is

$$\delta n = 1.316 \times 10^{-2} N \chi^{(3)}(\omega)(P/A). \quad (56)$$

Again we require $\delta(\Delta k)L \leq \pi$, and thus

$$\delta n \leq \frac{\lambda}{6L}. \quad (57)$$

Values of $\chi^{(3)}(\omega)$ for 1.064- and 0.6943-μ upconversion are given in the first column of Table IX. The second column gives the power density that will cause difficulty according to the criterion of (57). An atom density of 10^{16} atoms/cm^3 and a cell length of 1 m are assumed. Positive values of $\chi^{(3)}(\omega)$ indicate self-focusing (as opposed to defocusing) and will probably not cause a reduction in third-harmonic efficiency.

V. OPTIMIZATION

If limiting processes are neglected, the third-harmonic conversion efficiency [(17) and (18)] varies as the square of

TABLE X
LIMITING ATOM DENSITIES FOR TRIPLING—PHASE MATCHING BY MIXING WITH XE IS ASSUMED
(N IN ATOMS/cm^3, L IN cm, J/A IN J/cm^2, P/A IN W/cm^2)

Element	N Single-Photon Absorption (ω)	N Single-Photon Absorption (3ω)	N Two-Photon Absorption	N Kerr Effect	N Phase Matching
			1.064–0.3547 μ		
Li	$5.8 \times 10^{18}/L^{1/2}$	$7.3 \times 10^{18}/L^{1/2}$	$1.78 \times 10^{25}(A/LP)^{1/2}$	$1.88 \times 10^{30}(A/LP)$	$7.95 \times 10^{17}(A/LJ)^{1/2}$
Na	$7.6 \times 10^{18}/L^{1/2}$	$4.7 \times 10^{18}/L^{1/2}$	$1.26 \times 10^{25}(A/LP)^{1/2}$	$1.39 \times 10^{30}(A/LP)$	$1.05 \times 10^{18}(A/LP)^{1/2}$
K	$1.7 \times 10^{18}/L^{1/2}$	$2.7 \times 10^{18}/L^{1/2}$	$1.05 \times 10^{24}(A/LP)^{1/2}$	$7.89 \times 10^{28}(A/LP)$	$1.63 \times 10^{17}(A/LJ)^{1/2}$
Rb	$1.5 \times 10^{18}/L^{1/2}$	$1.3 \times 10^{18}/L^{1/2}$	$1.63 \times 10^{23}(A/LP)^{1/2}$	$1.88 \times 10^{28}(A/LP)$	$1.24 \times 10^{17}(A/LJ)^{1/2}$
Cs	$7.1 \times 10^{17}/L^{1/2}$	$1.7 \times 10^{18}/L^{1/2}$	$3.68 \times 10^{22}(A/LP)^{1/2}$	$6.01 \times 10^{27}(A/LP)$	$4.65 \times 10^{16}(A/LJ)^{1/2}$
			0.6943–0.2314 μ		
Li	$2.6 \times 10^{17}/L^{1/2}$	$1.2 \times 10^{17}/L$[a]	$1.19 \times 10^{23}(A/LP)^{1/2}$	$2.71 \times 10^{28}(A/LP)$	$1.30 \times 10^{16}(A/LJ)^{1/2}$
Na	$2.5 \times 10^{18}/L^{1/2}$	$3.8 \times 10^{18}/L$[a]	$1.87 \times 10^{23}(A/LP)^{1/2}$	$1.33 \times 10^{28}(A/LP)$	$2.4 \times 10^{17}(A/LJ)^{1/2}$

[a] Continuum loss: cross section assumed independent of N.

susceptibility, power density, cell length, and density of atoms. The maximum incident power density is determined by multiphoton ionization and is in the range of 10^{10}–10^{12} W/cm^2 for tripling in the alkali metals. For confocal focusing in a cell of length L ($A = L\lambda/4$), the length of the cell is an invariant with regard to conversion efficiency. For a laser with a given peak input power the cell should be chosen sufficiently long that with confocal focusing, the multiphoton ionization power density is not exceeded. For high-power lasers this may not be possible unless multipass techniques are employed. The limit on the maximum atom density is now determined by the most severe of the following: single-photon absorption at the fundamental, single-photon absorption at the third harmonic, two-photon absorption, Kerr effect, or, as will most often be the case, by the requirement that the incident energy density not destroy the phase-matching condition. Table X gives the value of the maximum atom density as determined by each of the above processes for tripling of 1.064- and 0.6943-μ radiation. The limit for each process is calculated assuming xenon phase matching at the required ratio. Laser pulses of length shorter than the atomic decay or quenching time are assumed.

As an example, assume an incident 1.064-μ pulse with a peak power of 10^8 W and a pulse length of 10^{-11} s. Assume that Na is to be used for tripling and that $P/A = 10^{11}$ W/cm^2 is the maximum power density allowed by multiple-photon (five) ionization (Table VII). For a 50-cm path length, the confocal area at 1.064 μ is 1.36×10^{-3} cm^2 and thus confocal focusing is just possible. From Table X, the maximum atom densities as determined for each of the limiting processes are as follows: single-photon absorption at (ω), $N_{max} = 1.07 \times 10^{18}$ atoms/cm^3; single-photon absorption at (3ω), $N_{max} = 6.65 \times 10^{17}$ atoms/cm^3; two-photon absorption, $N_{max} = 6.5 \times 10^{18}$ atoms/cm^3; Kerr effect, $N_{max} = 4.3 \times 10^{17}$ atoms/cm^3; and phase matching, $N_{max} = 1.71 \times 10^{17}$ atoms/cm^3. The most stringent tolerance is imposed by the joule tolerance on the phase-matching condition; and thus we take $N = 1.71 \times 10^{17}$ atoms/cm^3. At this pressure the cell is about 145 coherence lengths long and requires that temperature be constant to within about ± 0.6°C. For these conditions, (17) yields a conversion efficiency of 7.1 percent.

Table XI gives the maximum conversion efficiency, based on the joule limitation on the phase-matching condition, for each of the alkalies for 1.064- and 0.6943-μ third-harmonic generation. The first column assumes confocal focusing; thus cell length and area do not appear and the conversion efficiency depends only on the square of the incident power divided by the number of joules incident in an atomic decay time. The second column gives the maximum conversion efficiency in terms of incident power density, energy density, and cell length. The atom densities used to obtain these conversion efficiencies are given in the fourth column of Table X. The first column of Table XI applies under power-limited conditions. The second column applies once the limiting allowable power density is reached. For example, if we assume that five-photon ionization in sodium will allow a maximum incident power density of 1×10^{11} W/cm^2, then a 10-ps pulse (1 J/cm^2) in a 1-m-long cell will yield a conversion efficiency of 19 percent. Fig. 11 plots necessary power versus pulse length for 50-percent conversion.

VI. CONCLUSION

This paper has presented a theoretical study of third-harmonic generation in alkali metal vapors. Principal results of the analyses include the calculation of the third-order susceptibility as a function of wavelength for each of the alkalies, a derivation of the xenon buffer gas to alkali vapor mixing ratios required for phase matching, and a detailed study of the various limitations on efficient third-harmonic generation. It has been shown that the principal limitation process will be the breaking of phase matching caused by the change of the index of refraction due to absorption. Generally, lasers with 10-ps pulses will require 10^8–10^9 W peak power to achieve 50-percent conversion to the third harmonic.

A number of possibilities exist which may allow the energy density that may be passed through metal vapor

TABLE XI
MAXIMUM CONVERSION EFFICIENCIES AS LIMITED BY PHASE MATCHING

Element	Maximum Conversion Efficiency (Confocal Focusing-Power Limited)	Maximum Conversion Efficiency (Power Density Limited)
	1.064–0.3547 μ	
Li	$4.1 \times 10^{-22}(P^2/J)$	$1.09 \times 10^{-25}(P/A)^2L/(J/A)$
Na	$7.1 \times 10^{-21}(P^2/J)$	$1.89 \times 10^{-25}(P/A)^2L/(J/A)$
K	$7.6 \times 10^{-23}(P^2/J)$	$2.02 \times 10^{-27}(P/A)^2L/(J/A)$
Rb	$2.4 \times 10^{-20}(P^2/J)$	$6.38 \times 10^{-25}(P/A)^2L/(J/A)$
Cs	$1.3 \times 10^{-20}(P^2/J)$	$3.46 \times 10^{-25}(P/A)^2L/(J/A)$
	0.6943–0.2314 μ	
Li	$2.2 \times 10^{-24}(P^2/J)$	$3.82 \times 10^{-29}(P/A)^2L/(J/A)$
Na	$9.1 \times 10^{-22}(P^2/J)$	$1.58 \times 10^{-26}(P/A)^2L/(J/A)$

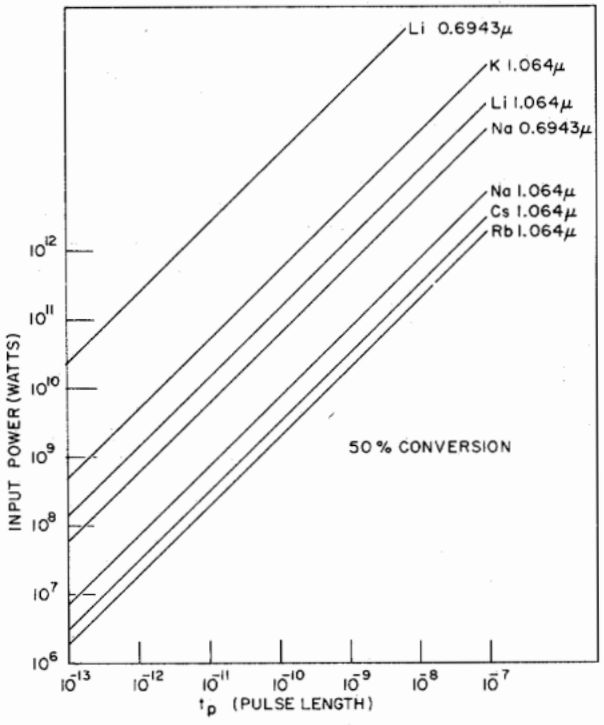

Fig. 11. Power necessary for 50-percent conversion versus pulse length for the alkalies.

tripling cells to be substantially increased. These include the following.

1) The reduction of the phase-matching ratio by replacing the inert gas with a media with higher refractive index per atom; for example Cd or Hg.

2) The use of a molecular quenching agent such as N_2 or H_2 to reduce the atomic decay time (for example, at ten atmospheres of nitrogen, the decay time of sodium is reduced by about a factor of 100 [30]; this should at least allow the use of a train of picosecond pulses instead of only a single pulse).

3) The use of multipass techniques combined with tight-focusing-type phase matching. This would allow operation at very low pressures with the associated natural linewidth, and as shown in Table VIII, yield very large saturation densities.

4) Finally, Bjorklund has suggested the use of discrete periodic phase matching. In this technique, cells of positively and negatively dispersive media are alternately spaced and their pressures independently adjusted. Here again, the metal vapor cell could be operated at very low pressure with very high energy saturation density.

The procedures developed in this paper can also apply to sequential third-harmonic steps further into the ultraviolet by the selection of other materials similar to those discussed, but having appropriate resonances in the ultraviolet rather than the visible spectral region. In recent months third-harmonic generation from 5320 to 1773 Å and from 3547 to 1182 Å has been obtained in cadmium and argon mixtures [29]. It is probable that this system has a significantly higher energy saturation density than does the alkali metal vapor system. It is possible to envision cascaded harmonic generators, possibly all within one heat pipe oven, leading to the generation of very short wavelengths. A four-stage system, for example, would yield 132 Å from a 1.064-m source. Although a system of this type would be complex, its output radiation will maintain many of the desirable features of the original radiation. It would thus be nearly diffraction limited, narrow band, polarized, and of picosecond duration.

ACKNOWLEDGMENT

The authors would like to express gratitude for many helpful discussions with A. E. Siegman, G. C. Bjorklund, A. H. Kung, and particularly J. F. Young. Experimental work done by the latter three was used to verify the theory, and the fine job of computer programming by L. B. Wigton was essential for the numerical results.

REFERENCES

[1] J. F. Ward and G. H. C. New, "Optical third harmonic generation in gases by a focused laser beam," *Phys. Rev.*, vol. 185, p. 57, 1969.
[2] J. A. Armstrong, N. Bloembergen, J. Ducuing, and P. S. Pershan, "Interactions between light waves in a nonlinear dielectric," *Phys. Rev.*, vol. 127, p. 1918, 1962.
[3] S. E. Harris and R. B. Miles, "Proposed third harmonic generation in phase-matched metal vapors," *Appl. Phys. Lett.*, vol. 19, p. 385, 1971.
[4] J. F. Young *et al.*, "Third harmonic generation in phase-matched Rb vapor," *Phys. Rev. Lett.*, vol. 27, p. 1551, 1971.
[5] L. I. Schiff, *Quantum Mechanics*, 3rd ed. New York: McGraw-Hill, 1968, p. 417.
[6] J. C. Slater, *Quantum Theory of Atomic Structure*. New York: McGraw-Hill, 1960, vol. I, ch. 6, vol. II, ch. 25.
[7] D. R. Bates and A. Damgaard, "The calculation of the absolute strengths of spectral lines," *Phil. Trans. Roy. Soc. London*, vol. A242, p. 101, 1949.
[8] H. B. Bebb, "Quantitative theory of the two-photon ionization of the alkali atoms," *Phys. Rev.*, vol. 149, p. 25, 1966.
[9] E. M. Anderson and V. A. Zilitis, "Oscillator strengths for sodium and potassium atoms calculated by a semiempirical method," *Opt. Spectrosc. (USSR)*, vol. 16, p. 99, 1964.
[10] —— "Semiempirical calculation of oscillator strengths for lithium, rubidium, and cesium atoms," *Opt. Spectrosc. (USSR)*, vol. 16, p. 211, 1964.
[11] J. Koch, "On the refraction and dispersion of the noble gases krypton and xenon," *Kungl. Fysiografiska Sallskapets I Lund Forhandlingar*, vol. 19, p. 173, 1949.
[12] W. H. Glenn, "Second-harmonic generation by picosecond optical pulses," *IEEE J. Quantum Electron.*, vol. QE-5, pp. 284–290, June 1969.
[13] S. Ch'en and M. Takeo, "Broadening and shift of spectral lines due to the presence of foreign gases," *Rev. Mod. Phys.*, vol. 29, p. 20, 1957.
[14] Landolt and Bornstein, *Zahlenwerte und Funktionen aus Physik*, vol. I, pt. 1, 6th ed. Berlin, Germany: Springer, 1950.
[15] W. L. Wiese, M. W. Smith, and B. M. Miles, N.B.S. Rep. NSRDA-NBS 22, vol. II, 1969.

[16] G. I. Goldberg, *Izv. Gl. Astron. Obser. Pulkove*, vol. 156, p. 126, 1956; results also given by Anderson [10].
[17] P. M. Stone, "Cesium oscillator strengths," *Phys. Rev.*, vol. 127, p. 1151, 1962.
[18] A. C. G. Mitchell and M. W. Zemansky, *Resonance Radiation and Excited Atoms*. New York: Cambridge, 1961.
[19] W. W. Houston, "Resonance broadening of spectral lines," *Phys. Rev.*, vol. 54, p. 884, 1938.
[20] R. W. Ditchburn, P. J. Jutsun, and G. B. Marr, "The continuous absorption of light in alkali-metal vapours," *Proc. Roy. Soc.*, vol. 219, p. 89, 1953.
[21] H. B. Bebb and A. Gold, "Multiphoton ionization of hydrogen and rare-gas atoms," *Phys. Rev.*, vol. 143, p. 1, 1966.
[22] V. M. Morton, "Multi-photon absorption in monatomic gases," *Proc. Phys. Soc.*, vol. 92, p. 301, 1967.
[23] H. Kogelnik and T. Li, "Laser beams and resonators," *Appl. Opt.*, vol. 5, p. 1550, 1966.
[24] K. Kishi, K. Sawada, T. Okuda, and Y. Matsuoka, "Two photon ionization of cesium and sodium vapors," *J. Phys. Soc. Japan*, vol. 29, p. 1053, 1970.
[25] Ya. B. Zel'dovitch and Yu. P. Raizer, "Cascade ionization of a gas by a light pulse," *Sov. Phys.——JETP*, vol. 20, p. 772, 1965.
[26] C. C. Wang and L. I. Davis, Jr., "New observations of dielectric breakdown in air induced by a focused Nd^{3+}-glass laser with various pulse widths," *Phys. Rev. Lett.*, vol. 26, p. 822, 1971.
[27] I. K. Krasyuk, P. P. Pashinin, and A. M. Prokhorov, "Investigation of breakdown in argon and helium produced by a picosecond ruby laser light pulse," *Sov. Phys.——JETP*, vol. 31, p. 860, 1970.
[28] J. E. Rizzo and R. C. Klewe, "Optical breakdown in metal vapours," *Brit. J. Appl. Phys.*, vol. 17, p. 1137, 1966.
[29] A. H. Kung, J. F. Young, G. C. Bjorklund, and S. E. Harris, "Generation of vacuum ultraviolet radiation in phase matched Cd vapor," to be published.
[30] P. K. Kibble, C. Copley, and L. Krause, "Inelastic collisions between excited alkali atoms and molecules. II. The quenching of sodium resonance radiation by N_2, H_2, HD, and D_2," *Phys. Rev.*, vol. 159, p. 11, 1967.

Properties of a Radial Mode CO_2 Laser

LEE W. CASPERSON AND CHARLES ROMERO

***Abstract*—The properties of a new class of lasers are investigated theoretically and experimentally. In these lasers, the radiation propagates radially within a disk-shaped amplifying medium resulting in high fields and symmetric illumination at the resonator axis. Experiments have been conducted using a pulsed CO_2 TEA configuration.**

I. Introduction

MOST conventional laser resonators consist of a pair of mirrors between which radiation propagates. If one or both of the mirrors are made spherical to reduce diffraction losses, then the resonator modes can be described by well-known Laguerre–Gaussian or Hermite–Gaussian functions. The subject of this paper is a new type of laser in which the radiation propagates radially within a wrap-around mirror like that shown in Fig. 1. An internal mirror concentric to the outside mirror can be added so that the z axis is external to the resonator. Among the important properties of these new lasers are the high fields and uniform illumination at the laser axis. The saturation behavior is much like that of other lasers, but the analytic expressions are all modified to account for the radial propagation. We report here the first operation of a radial mode laser. Our experiments have been conducted using for the amplifying medium a transverse-excitation atmospheric (TEA) discharge in a CO_2–He–N_2 gas mixture [1]. Output pulses are obtained at a wavelength of 10.6 μ with peak power of up to about 100 kW. The laser oscillates uniformly about its axis and the output properties are in good agreement with theory.

Manuscript received November 16, 1972. This work was supported in part by the National Science Foundation. Part of this paper was presented at the 25th Annual Gaseous Electronics Conference, London, Ont., Canada, October 1972.

L. W. Casperson is with the School of Engineering and Applied Science, University of California, Los Angeles, Calif.
C. Romero was with the School of Engineering and Applied Science, University of California, Los Angeles, Calif. He is now with the Electron Dynamics Division of Hughes Aircraft Company, Torrance, Calif. 90509.

II. Theory

In this section, the radial beam modes are discussed and the saturation behavior is obtained for the simplest case of steady-state oscillation. From the wave equation, one finds that the outward-propagating harmonically varying modes are described by the function [2]

$$\psi = \psi_0\left(\frac{w_0}{w}\right)^{1/2}\begin{Bmatrix}\sin\\ \cos\end{Bmatrix} m\phi H_m^{(2)}(kr) H_n\left(2^{1/2}\frac{z}{w}\right) \cdot \exp\left(-\frac{ikz^2}{2R} - \frac{z^2}{w^2} - iP_n\right), \quad (1)$$

where $w = w_0\,[1 + (r/r_0)^2]^{1/2}$ is the spot size in the z direction of the fundamental Gaussian mode, $r_0 = \pi w_0^2/\lambda$ is the Rayleigh length, $R = r[1 + (r_0/r)^2]$ is the radius of curvature in the z direction, $k = \omega(\mu\epsilon)^{1/2}$ is the propagation constant, $H_m^{(2)}$ is a Hankel function of the second kind, H_n is a Hermite polynomial, and $P_n = -(n + 1/2)\tan^{-1}(r/r_0)$ is the phase. A similar expression involving $H_m^{(1)}$ can be written for inward-propagating modes, or alternatively, the modes can be expressed in terms of the Bessel functions $J_m = [H_m^{(1)} + H_m^{(2)}]/2$. The wave function ψ may be interpreted as the z component of either the electric field or the magnetic field and the other field com-